Eur. Phys. J. A **3**, 183–195 (1998)

THE EUROPEAN PHYSICAL JOURNAL A

Backward slow protons production in the inelastic interactions of ^{6}Li and ^{7}Li nuclei with emulsion nuclei at Dubna energy

M. El-Nadi[1], A. Abdelsalam[1], N. Ali-Mossa[2], Z. Abou-Moussa[1], S. Kamel[1], Kh. Abdel-Waged[3a], W. Osman[1], B. Badawy[1]

[1] Physics Department, Faculty of Science, Cairo University, Egypt
[2] Basic Science Department, Faculty of Engineering, Shoubra, Egypt
[3] Physics Department, Faculty of Science, Benha University, Egypt (E-mail: Khelwagd@frcu.eun.eg)

Received: 25 August 1997 / Revised version: 5 May 1998
Communicated by C. Signorini

Abstract. We report the experimental measurements on the multiplicity of slow target associated particles, in the forward ($\theta_{lab} \leq 90^\circ$) and backward ($\theta_{lab} > 90^\circ$) hemispheres, and the different correlations between the backward slow protons and the production of hadrons in both hemispheres in the interactions of ^6Li(3.7 A GeV) and ^7Li(2.2 A GeV) with emulsion nuclei. The study of the number of backward slow protons (N_b^b and N_g^b) indicates that while the number of backward black particles, N_b^b, is a good factor representing the purely target fragments, the number of backward grey particles, N_g^b, can be considered as an accurate experimental factor for the impact parameter dependence of the collision. It is also shown that the most central collisions are events having $N_g^b > 0$ and $N_s^b > 0$. We confront the data with a multiple scattering model incorporating both binary cascading and evaporation of residual nucleus. The model applies well in the region of limited cascading (backward hemisphere). As for the forward hemisphere, where cascading becomes more branched, the model becomes less applicable.

PACS. 25.70.Mn Projectile and target fragmentation – 25.75.-q Relativistic heavy-ion collisions

1 Introduction

One of the important aspects in nucleus-nucleus (AA) interactions is the emission of pions and protons in the backward hemisphere (BHS) ([1]- [10]). In free nucleon-nucleon (NN) collisions, the hadron emission in the BHS is kinematically restricted. The emission of hadrons beyond the kinematic limit may be an evidence for exotic production mechanisms. Therefore, the emission of such hadrons in heavy ion-collisions in the BHS supplies interesting information on nuclear effects such as the interaction of hadrons from the primary interaction zone with the surrounding nuclear matter, the internal nucleons motion inside the nucleus and short range correlation between nucleons.

The present work is a continuation of our program of studying the backward particle production in the interactions of various projectiles with emulsion nuclei at Dubna energy. Here we report the experimental data on the various characteristics of the events emitting backward protons ($\theta_{lab} > 90^\circ$) in the interactions of ^6Li(3.7 A GeV) and ^7Li(2.2 A GeV) nuclei with nuclear emulsion. The different correlations between the production of slow protons in the backward and forward ($\theta_{lab} \leq 90^\circ$) hemispheres are also studied.

The collected data are analyzed in the framework of the intra-nuclear cascade model coupled with the classical evaporation model ([11]- [13]). Within this combined model (in short, the Cascade Evaporation Model (CEM)), the high energy projectile undergoes a multiple scattering process with the nucleons of the target nucleus. The cascade of created secondaries with the nucleons of the target (and projectile) contribute significantly to particle production in the target (and projectile) fragmentation regions. We apply this simple superposition model to the data to disentangle any events (in the backward or forward (FHS) hemispheres) that might be an evidence of a collective behavior.

The paper is organized as follows: In Sect. 2 we demonstrate the experimental techniques and the selection criteria. In Sect. 3 we review the basic ideas of the CEM. Sect. 4 contains the discussion of the experimental results on the basis of CEM. Finally in Sect. 5 we summarize the conclusions that can be drawn from the paper.

[a] Author to whom all correspondence should be addressed

2 Experimental procedures

In this experiment, two photoemulsion stacks consisting of $BR-2$ pellicles are used. These pellicles were exposed horizontally to ^6Li and ^7Li ions with energy 3.7 A GeV and 2.2 A GeV, respectively, at Dubna Synchrophasotron, Russia. The thickness of each pellicle is 600 μm with a sensitivity of about 30 grains per 100 μm for the minimum ionizing particles. The composition of the used emulsion is represented in Table 1. Each pellicle was doubly scanned by along the track scanning method, fast in the forward direction and slow in the backward one using a total magnification of about 1500×. Data studied in the present work consist of 1021 and 1011 inelastic interactions of ^6Li and ^7Li with emulsion nuclei, respectively. The general characteristics and other details on our experiments have been published before ([14–16]).

In all inelastic events, the emitted charged secondaries were classified according to the general criteria as:

- Shower particles: They are the singly charged relativistic particles produced, with kinetic energy $K.E >$ 400 MeV, outside the projectile fragmentation cone ($\theta_{cone} = 3.2°$, 4.6° for ^6Li and ^7Li, respectively) with relative ionization ($I/I_0 \leq 1.4$), where I_0 is the plateau ionization for the singly charged minimum ionizing particles. They are mainly charged pions with velocity $\geq 0.7c$. Their multiplicity is denoted by N_s.
- Grey particles: Which are the charged particles of relative ionization ($1.4 < I/I_0 < 10$) and a range ≥ 3 mm in emulsion. These particles are mainly protons with kinetic energy in the range of (26 − 400 MeV). Their multiplicity is denoted by N_g.
- Black particles: They are the charged particles with ($I/I_0 \geq 10$) and a range < 3 mm in emulsion. They are mainly the evaporation products of the remnant of the target nucleus which are characterized by $K.E <$ 26 MeV. Their multiplicity is denoted by N_b. In each event the black and the grey particles are called heavily ionizing particles. They are mainly target fragments and their multiplicity is denoted by N_h.
- Projectile fragments: Referred to the spectator nucleons of the projectile with velocity $\simeq 0.97c$ emitted inside the forward fragmentation cone. In our case they are singly or doubly charged fragments. The single charged fragments emitted in the fragmentation cone were subjected to rigorous multiple scattering measurements for the momentum determination in order to separate the produced pions from them. In each event the total charge of the projectile spectators Q =[The number of $Z = 1$ + the number of $Z = 2$ charged fragments in the fragmentation cone] was estimated.

Table 1. The chemical composition of $BR-2$ emulsion

Element	^1_1H	$^{12}_6C$	$^{14}_7N$	$^{16}_8O$	$^{80}_{35}Br$	$^{108}_{47}Ag$
$\frac{No.of atoms}{c.c\times 10^{22}}$	3.150	1.412	0.395	0.956	1.028	1.028

3 Model prescriptions

In this section we outline the basic ideas of the model and summarize the most important features.

(i) Initially, the positions of the nucleons of the two colliding nuclei (A and B) are sampled according to oscillator densities distribution for A, $B \leq 10$ and the Saxon-Wood density for heavier nuclei, with parameters $R_A = 1.07$ $A^{1/3}$ fm and $c = 0.545$ fm. In choosing the nucleon coordinates, the nucleon core is included (No two nucleons can be closer than R_c, $R_c = 0.4$ fm). In each nucleus, the nucleon momenta are sampled according to zero-temperature Fermi-distributions:

$$\frac{dN_i}{dp} = 3p^2 \left(\frac{N_i}{(p_i^f)^3}\right), \tag{1}$$

where i = neutron (n) or proton (p). The maximum allowed Fermi momenta of neutrons and protons are

$$p_i^f = \left[\frac{3h^3}{8\pi}\frac{N_i}{V_A}\right]^{1/3},$$

where $N_p = Z$, $N_n = A - Z$, V_A stands for the volume of the corresponding nucleus with radius R_A (Note that $N_i/V_A = \rho_A(r)$ is the density of the nucleus A).

(ii) The nuclei are given their initial momenta by Lorentz boosting. Their shapes are accordingly Lorentz contracted.

(iii) The scattering process is described by a succession of binary scatterings among the constituent nucleons. To be more specific, the collision proceeds via n elementary interactions between n_p and n_t nucleons from the projectile and target, respectively. The values n, n_p and n_t are sampled according to Glauber's multiple scattering formalism using the MC algorithm of Ref. [17]. The nucleons which participate in the interaction accept momentum and begin to move in the nucleus. A pair of particles (i, j) could collide if:

$$(b_x + x_i - x_j)^2 + (b_y + y_i - y_j)^2 \leq (R_{int} + \lambda_D)^2,$$

where $b_{x,y}$ and $x_{i,j}$, $y_{i,j}$ are the components of the impact parameter vector and the coordinates of the pair, respectively. R_{int} is the strong interaction radius (1.3 fm) and λ_D is the de Broglie wavelength of the nucleon. Once the scattering takes place (whether it is elastic or inelastic) the probabilities are determined randomly according to:

$$P_{el} = \sigma_{el}/(\pi \times (R_{int} + \lambda_D)^2),$$

$$P_{in} = \sigma_{in}/(\pi \times (R_{int} + \lambda_D)^2),$$

where σ_{el} and σ_{in} are the elastic and inelastic NN-cross sections, respectively.

(iv) The momenta of the colliding particles are determined randomly according to the experimental differential cross section. After the first NN-collision has been completed, straight line motion is resumed and the next possible collision is followed in a similar manner and so on. The sequence of the two body collisions is followed until

the cascade nucleon either escapes from the nucleus or its kinetic energy within the nucleus falls below the Fermi energies.

Several features are added to this simple picture. First, the nucleons of a nucleus of mass number A and charge Z move in an effective nuclear potential defined by a sum of a Fermi-potential and a binding energy contribution:

$$V_i(A,Z) = \frac{[p_i^f(A,Z)]^2}{2m_i} + E_i^{bind}(A,Z), \qquad (2)$$

where m_i is the nucleon mass. For a positively charged particle a Coulomb term, V_c, must be added to (2). Thus for a nucleon leaving the nucleus A, its energy must exceed the effective nuclear potential (2) and in case of a proton it has to overcome the Coulomb barrier. Second, Pauli principle is included by suppressing collisions in which the final momentum of one of the two colliding nucleons lies below the Fermi momentum. Third, the pion production is introduced by considering the inelastic NN-cross section. Fourth, the so-called trailing effect (rearranging the density) is included; when, for example, a target nucleon is scattered as a result of being collided with the projectile, the whole target density is depleted by one nucleon.

Following the completion of the cascade process, the masses of the residual nuclei are determined by product nucleons that have not been escaped from the nuclei. Product mesons that have not escaped from the nuclei are taking into account in determining the charges of residual nuclei.

The excitation energy of a residual nucleus is given by the sum of the energies absorbed by the corresponding nucleus and the energies of holes formed in the process. It is assumed that due to interaction of a projectile nucleon (or a cascade particle) with a target nucleon (having the energy $p^2/2m_i$), a hole with an energy $E_h = (p_i^f)^2/2m_i - p^2/2m_i$ is created in the target nucleus. If an energy T of a nucleon after the interaction is greater than the Fermi energy but still lower than V_i the nucleon will be absorbed with an energy $E_n = T - (p_i^f)^2/2m_i$. A meson of mass m_π having an energy T_π lower than 25 MeV is considered as an absorbed one too. Its contribution to the excitation energy is given by $T_\pi + m_\pi$. Thus the total excitation energy of the nucleus is the sum of the energies of the holes and energies of absorbed nucleons and mesons.

After the termination of the cascade stage, the nuclear residues are not necessarily in thermodynamic equilibrium. The process leading to the formation of thermalized residual nuclei is accompanied by equilibrium particle emission. This process occurs if the number of particles in the residual nucleus, $N_q = N_n + N_h$, is greater than the equilibrium value $N_q(Eq.) = \sqrt{6aE^*/\pi^2}$. Here N_h is the number of holes, N_n is the number of captured cascade nucleons, E^* is the excitation energy of the residual nucleus and a is the parameter of the level density in the nucleus ($a = A/10$ MeV^{-1}). Pre-equilibrium decay was simulated on the bases of pre-equilibrium exciton model [18].

At the end of the cascade process the nuclear residue are supposed to be left in an equilibrium state characterized by their masses, charges and excitation energies. Nucleons and light fragments (α, d, ^3H, ^3He) would be emitted if the excitation energy of the residual nucleus is higher than the separation energy. The emission process can be described as an evaporation from a hot system. The treatment starts from the formula of Weisskopf ([13], [19]) in an application of the detailed balance.

The evaporation probability for a particle of type (j), mass m_j spin s_j and kinetic energy E is given by

$$P_j(E)dE = \frac{(2s_j+1)m_j}{\pi^2\hbar^3}\sigma_{inv}\frac{\rho_f(U_f)}{\rho_i(U_i)}EdE \qquad (3)$$

where ρ's are the nuclear level densities ($\rho_f(U_f)$) for the final nucleus, $\rho_i(U_i)$ for the initial one, U_i is the excitation energy of the evaporating nucleus, $U_f = U - E - Q_j$ of the final one, Q_j is the Q value for emitting a particle of type (j) and σ_{inv} is the inverse cross section for the inverse process.

In the original work of Dostrovosky [20],

$$\rho(U) \simeq Ce^{2\sqrt{aU}},$$

The inverse reaction cross section has been parameterized in a simple way so that expression (3) can be analytically integrated and used for MC sampling.

The parameters of the model were determined as a result of an analysis of hA-interactions ([21]- [22]). We do not change these values in our calculations.

Photoemulsions contain hydrogen, carbon, nitrogen, oxygen, bromine and silver. We generated 5000 simulated events for the interaction of each projectile nucleus with the different nuclei of emulsion.

In order to investigate the probability of having superposition of projectile reactions induced on light and heavy emulsion nuclei, the multiplicity distribution of heavily ionizing tracks ($P(N_h)$) as a result of interactions of ^6Li with light (CNO) and heavy ($BrAg$) components of emulsion nuclei were calculated. In Fig. 1a we show these calculations where it demonstrates that the probabilities of the interaction with light nuclei is quite different from those with heavy nuclei. The N_h-distribution due to the interactions with CNO nuclei extends to $N_h \sim 7$. At $N_h > 7$ the distribution falls off rapidly to zero. However, the distribution due to the interactions with $BrAg$ nuclei is flattened in the whole N_h range. It is also to be noticed that in the region $1 \leq N_h \leq 7$, the distribution is contaminated by the interaction with the $BrAg$ nuclei. At $N_h > 7$ the interactions with $BrAg$ nuclei become dominant.

As an example, we show in Fig. 1b the impact parameter dependence on the N_h values, where one can see in the region $1 \leq N_h \leq 7$ the impact parameter rapidly decreases with increasing N_h values. At $N_h > 7$, the impact parameter becomes nearly constant; this is because the wide range of impact parameters within the $BrAg$ nuclei gives rise to collisions in which the projectile interacts with a nearly constant number of target nucleons.

From the point of view of modern approaches, ([23]- [26]) this version of the CEM model disregards many important effects such as the production of mesonic and

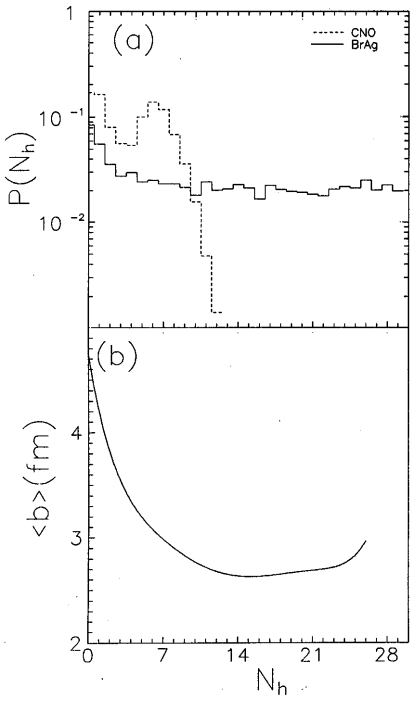

Fig. 1. a The multiplicity distribution of heavily ionizing particles for $^6Li + Em$ at 3.7 AGeV due to interaction with CNO components (*dashed line*) and $BrAg$ components (*solid line*) of nuclear emulsion. **b** The average impact parameter dependence on N_h values

baryonic resonances, the finite time of secondary particle formation, variations in the mean nuclear field and the coalescence of nucleons. The calculations of product particles and correlations between slow and fast particles are expected to be sensitive to these details. To clarify the key problems encountered in the description of these features in the FHS and BHS, we consider that it is convenient to use this simplified approach as a first approximation.

Below, we consider the conclusions that can be drawn from comparison between the present experimental data and the results of our calculations.

4 Results and discussion

As already mentioned, hadrons produced in AA-interactions at high energy may originate from two mechanisms. They may participate only in the primary reaction and leave the overlap region of projectile and target without further interactions. In emulsion experiments such hadrons are seen as shower tracks (s-particles). Or they may be involved in the rescattering process- by knocking out further nucleons while penetrating through the spectator parts of the nuclei. The intranuclear cascade is responsible for knocking out cascade protons and neutrons of the spectator fragments. Most of the cascade protons have energies typical for the so-called grey prongs (g-particles).

Both the primary and secondary NN-interaction contribute to the excitation of the spectator fragments. In peripheral AA-interaction the de-excitation of the residual nuclei proceeds via evaporation of nucleons and light fragments (d, ^3H, ^3He, α) until a stable configuration is reached. In emulsion such particles are seen as black tracks (b-particles).

The group of b-particles is dominated by protons which is considered as the product of evaporation of residual nuclei at the latter stage of the interaction. There are also many protons among g-particles. These protons are assumed to be produced at the first fast stage of the interaction. The group of s-particles contain primarily product mesons. Thus the observed correlations between the multiplicities of s, g and b-particles reflect the interplay between the fast and slow stages of the interaction.

In the next subsections, we are going to investigate the source of backward slow protons, their target size and impact parameter dependencies and the different correlations between the backward and the forward slow protons.

4.1 Dependence of the backward protons on target size and projectile energy

Table 2 shows the probability of observing events accompanied by a backward g-particles ($N_g^b > 0$) in the interactions of ^6Li(3.7 A GeV) and ^7Li(2.2 A GeV) with emulsion nuclei. The probability of interactions associated with backward emission of g-particles for two different target sizes ($1 \leq N_h \leq 7$ and $N_h \geq 8$) are also presented. The group of events having $1 \leq N_h \leq 7$ belongs to both CNO collisions and peripheral $BrAg$ collisions whereas the $N_h \geq 8$ group is due to interactions with quasi-central or central with $BrAg$ nuclei. In order to separate the events due to CNO from those due to $BrAg$ in the region $1 \leq N_h \leq 7$, the method of Florian et al [27] is used according to which it is found that in this region 63% and 37% of the events are due to interaction with light and heavy emulsion nuclei, respectively. Therefore, it is possible to get events belonging to $BrAg$ and having small values of N_g or N_b. The data of these events are included in our representation.

It is interesting to notice that in case of the group of events having $N_h \geq 8$, the number of events accompanied by the emission of g-particles in the BHS is nearly four times larger than those in case of the group of interactions having $1 \leq N_h \leq 7$.

Therefore the emission of backward g-particles (mainly protons) depends on the target size. In the same table, it is observed that the percentage of events accompanied by

Table 2. The percentage of the number of events accompanied by a backward g-particles in the interactions of ^6Li and ^7Li with emulsion nuclei and at different target sizes ($N_h \leq 7$ and $N_h \geq 8$)

Projectile	Energy	Total sample	Total	$N_h \leq 7$	$N_h \geq 8$
^6Li	3.7 A	1021	47.00	23.47	86.10
^7Li	2.2 A	1011	34.42	18.65	65.87

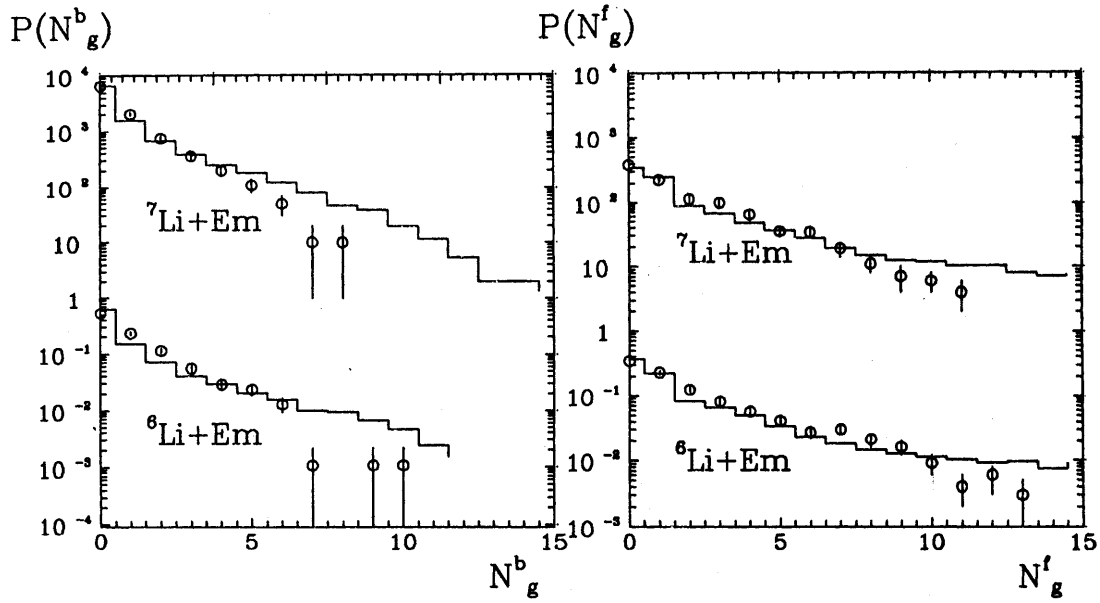

Fig. 2. Multiplicity distributions of forward (right) and backward (left) g-particles in the interactions of ^6Li(3.7 A GeV) ^7Li(2.2 A GeV) with nuclei of photoemulsion: histograms denote CEM calculations and (points) represent the experimental data. For $^7Li + Em$, both experimental data and calculations are multiplied by a factor of 10^4

grey protons emitted in the BHS in case of ^6Li(3.7 A GeV) interactions is higher than in case of interactions induced by ^7Li(2.2 A GeV). These results are consistent with those in Ref. [28], where they observed that the probability of events accompanied by the emission of backward protons increases with increasing the energy.

4.2 Multiplicity distribution of forward-backward slow protons

Figure 2 illustrates the multiplicity distributions of g-particles in the forward ($P(N_g^f)$) and the backward ($P(N_g^b)$) hemispheres for ^6Li(3.7 A GeV) and ^7Li(2.2 A GeV) interactions with emulsion together with CEM calculations.

In our calculations we have normalized the distributions to unity and apply the previously given definition for the forward and backward g-particles. The results of the calculations completely agree with the measured distributions apart from a possible overestimation of the tail of $N_g^{f,b}$ distributions at high multiplicities. The calculated g-particle distributions in the FHS for $N_g^f > 7$ differ from the measured ones in that they tend to be flat. This indicates that the theoretical calculations involve more cascading than what is really experimentally occurred. The situation is reversed in the BHS, where the data show a flat distribution for $N_g^b \geq 7$ while the calculated probability of backward g-particles decreases with increasing N_g^b. This may reflect that the production mechanisms of g-particles in the two hemispheres are different.

Figure 3 presents the multiplicity distributions of b-particles in the forward ($P(N_b^f)$) as well as the backward ($P(N_b^b)$) hemispheres for the reactions under study. In our calculations the distributions are normalized to unity and we apply the definition for b-particles as those singly and multiply charged particles having lower energies than the g-particles.

Except for $^7Li + Em$ in the FHS, the calculations agree with the measured distributions for $N_b^{f,b} \geq 7$.

This indicates that the evaporation model used is quite successful in explaining the evaporation of heavy residual nuclei. For light nuclei ($N_b^{f,b} < 7$), the sequential emission scheme underlying the classical evaporation model used becomes less and less applicable and we observed fewer evaporated particles than the measured values. Therefore, other de-excitation mechanisms are more suitable for these light residual nuclei. We think that the Fermi break-up model [29] should be adopted in this region. In this model, the excited nucleus is supposed to disassemble in one step into two or more fragments. Thus more and more evaporated particles will be produced from light nuclei and thus filling the region $N_b^{f,b} < 7$.

4.3 Average multiplicities of forward-backward slow protons

In Table 3 we present the data obtained on the mean values of the g- and b-particles emitted in the forward and backward hemispheres and the forward to backward ratios, $(F/B)_{g,b}$. The calculated values of the average multiplicities are also given in parenthesis. From the analysis of the above results one notices that:

- The average values of g- and b-particles increase with increasing target size (N_h values).
- The $(F/B)_g$ ratio decreases with increasing target size.

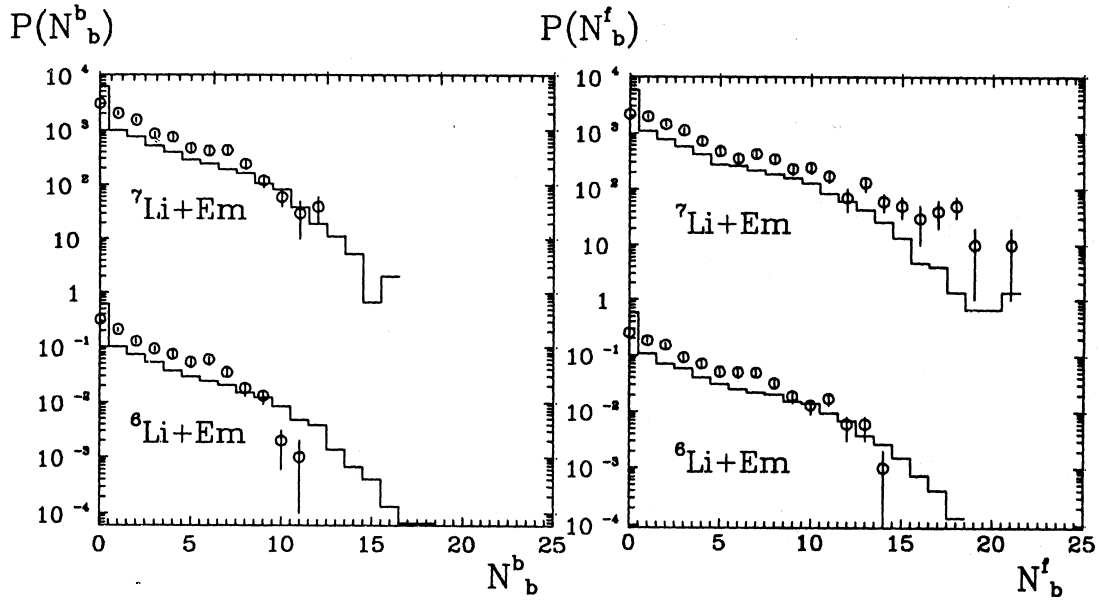

Fig. 3. Multiplicity distributions of forward (right) and backward (left) b-particles in the interactions of the two lithium isotopes with emulsion nuclei. For $^7Li + Em$, both experimental data and calculations are multiplied by a factor of 10^4. The notations are the same as in Fig. 2

Table 3. The values of the total average multiplicities of the emitted slow particles in the forward and backward hemispheres, the average multiplicities of different target sizes ($1 \leq N_h \leq 7$ and $N_h \geq 8$) and the forward-backward ratios $(F/B)_{g,b}$, for $^6Li + Em$ and $^7Li + Em$ interactions. The corresponding CEM results are given in parentheses

^6Li	$< N_g^f >$	$< N_g^b >$	$< N_b^f >$	$< N_b^b >$	$(F/B)_g$	$(F/B)_b$
Total	2.08 ± 0.08 (3.163)	0.98 ± 0.05 (1.05)	2.84 ± 0.09 (1.795)	2.19 ± 0.07 (1.438)	2.15	1.29
$1 \leq N_h \leq 7$	0.67 ± 0.02 (1.461)	0.28 ± 0.03 (0.376)	1.01 ± 0.06 (0.704)	0.79 ± 0.04 (0.512)	2.40	1.28
$N_h \geq 8$	4.42 ± 0.20 (9.221)	2.12 ± 0.08 (3.215)	5.86 ± 0.21 (5.437)	4.52 ± 0.11 (4.437)	2.08	1.30
^7Li						
Total	1.77 ± 0.07 (2.893)	0.64 ± 0.04 (0.840)	3.38 ± 0.12 (1.744)	2.29 ± 0.08 (1.391)	2.78	1.48
$1 \leq N_h \leq 7$	0.70 ± 0.04 (1.455)	0.24 ± 0.02 (0.303)	1.27 ± 0.07 (0.697)	0.88 ± 0.04 (0.505)	3.37	1.44
$N_h \geq 8$	3.69 ± 0.18 (8.311)	1.35 ± 0.08 (2.622)	7.27 ± 0.29 (5.322)	4.92 ± 0.13 (4.333)	2.73	1.48

- The $(F/B)_{g,b}$ ratios of g- and b-particles in both hemispheres in case of the interactions induced by ^7Li are higher than in case of the interactions with ^6Li.
- The number of g-particles emitted in the FHS is higher than the number of particles emitted in the BHS. This result is reflected on the values of forward to backward ratio $(F/B)_g$. This ratio is seen to depend on the projectile mass number as well as on the target size. Its values lie in the range $(F/B)_g = 2.2 - 2.8$. The $(F/B)_g$ ratio represents the anisotropy ratio of the angular distribution:

$$(F/B) \simeq \exp[(4/\sqrt{\pi})\beta_{\|}/\beta_0] \qquad (4)$$

where $\beta_{\|}$ is the mean longitudinal velocity of the center of mass of the emitting system and $\beta_0 = 0.35$ is the characteristic velocity of the system (taken from Ref. [30]). By substituting in (4) with the values of the anisotropy ratio $(F/B)_g$ and β_0, we obtain $\beta_{\|} = 0.12 - 0.16$. This gives the temperature of the emitted system $T = M\beta_{\|}/2 \sim 58$ MeV, where M is the nucleon mass.
- In the case of b-particle, the forward-backward ratio $((F/B)_b = 1.3 - 1.5)$ slightly depends on the projectile and target sizes. Similar to what we have done for g-particles, the system emitting b-particles moves relatively slow and has a spectral velocity $\beta_0 \simeq 0.115$. This gives the average velocity of this system $\beta_{\|} = 0.015$ and therefore its temperature equals 7 MeV. Thus the target fragmentation has two temperatures; one for b-particles (7 MeV) and another (58 MeV) for g-particles.

- The calculated $< N_g^f >$ as a function of $1 \leq N_h \leq 7$ or $N_h \geq 8$ is nearly twice the corresponding measured values.
- The CEM predictions slightly exceed the measured $< N_g^b >$ over different target sizes.
- While the calculated $< N_b^{f,b} >$ are less than the observed values for light nuclei evaporation ($1 \leq N_h \leq 7$), there are no significant differences for the evaporation of the heavy nuclei ($N_h \geq 8$).

4.4 Target size dependence

In Fig. 4, we study the effect of target size on the multiplicity of outgoing protons emitted in the fast stage of the interaction (and detected as g-particles) in the two hemispheres. One can see that:

- Experimentally, the dependence of the mean number of g-particles ($< N_g^{f,b} >$) on N_h increases with increasing the energy of the projectile.
- In contrast to the measured correlations, the calculated ones show a bump near $N_h \sim 8$. This bump separates the interactions which are mostly with light nuclei from those with the heavy ones.
- The calculations agree with the mean number of backward grey $< N_g^b >$ as a function of N_h. On the other hand, the calculated average values of forward g-particles ($< N_g^f >$) as a function of N_h exceed the measured correlations.

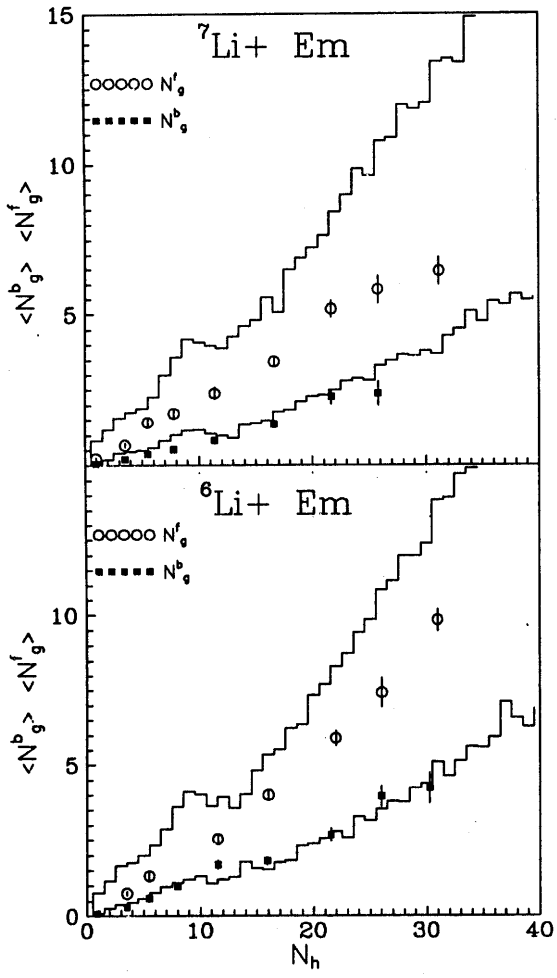

Fig. 4. The correlations between forward-backward (N_g^f, N_g^b) g-particles and N_h multiplicities

A natural way to reach an agreement in the FHS with experimental data is to suppress cascading. There are two factors which affect the yield of g-particles and are disregarded in the model used here. These are the coalescence of nucleons (that is, the formation of light nuclear fragments from nucleons that are close in phase-space) and the absorption of pions by two nucleon pairs. The former can reduce the absorption of g-particles, while the latter can increase it. The importance of these factors grows with increasing the multiplicity of particles and becomes much more pronounced in the FHS.

Next we study the effect of target size on the particles emitted from the slow stage of the interaction both in the forward and backward directions. In Fig. 5 we present the dependence of the average values of b-particles in the two hemispheres $< N_b^{f,b} >$ on N_h. According to the model, the yield of b-particles is determined by the excitation energy of the residual nuclei and by the evaporation effects. An increase of N_h-particles from $0 - 15$ is accompanied by a fast increase in the multiplicity of b-particles. This is due to the superposition of the characteristics of two group of events with small and large multiplicity of b-particles.

In the BHS the dependence of $< N_b^b >$ on N_h is slightly underestimated by the model for the two lithium isotopes interactions. In contrast to the measured correlations in the FHS, the calculated ones show a weaker dependence of the average forward b-particles ($< N_b^f >$) on $N_h > 15$.

4.5 Impact parameter dependence

In order to study the dependence of the observed multiplicity of the emitted g- and b-particles in the forward and backward hemispheres on the projectile spectators, we divide our data into subgroups characterized by different values of the projectile spectators Q [$Q = 0, 1, 2$]. The Q-values characterize the degree of centrality which can be related to the impact parameter. In Tables 4 and 5 we present the multiplicity characteristics of the target fragments (g- and b-particles) at different values of Q together with the model predictions. From the above data we notice that:

- The mean values of the emitted target fragments decrease with increasing the projectile spectator (increasing impact parameter) in both hemispheres. This holds for both measurements and calculations.
- Concerning the experimental $(F/B)_{g,b}$ ratios one observes that:

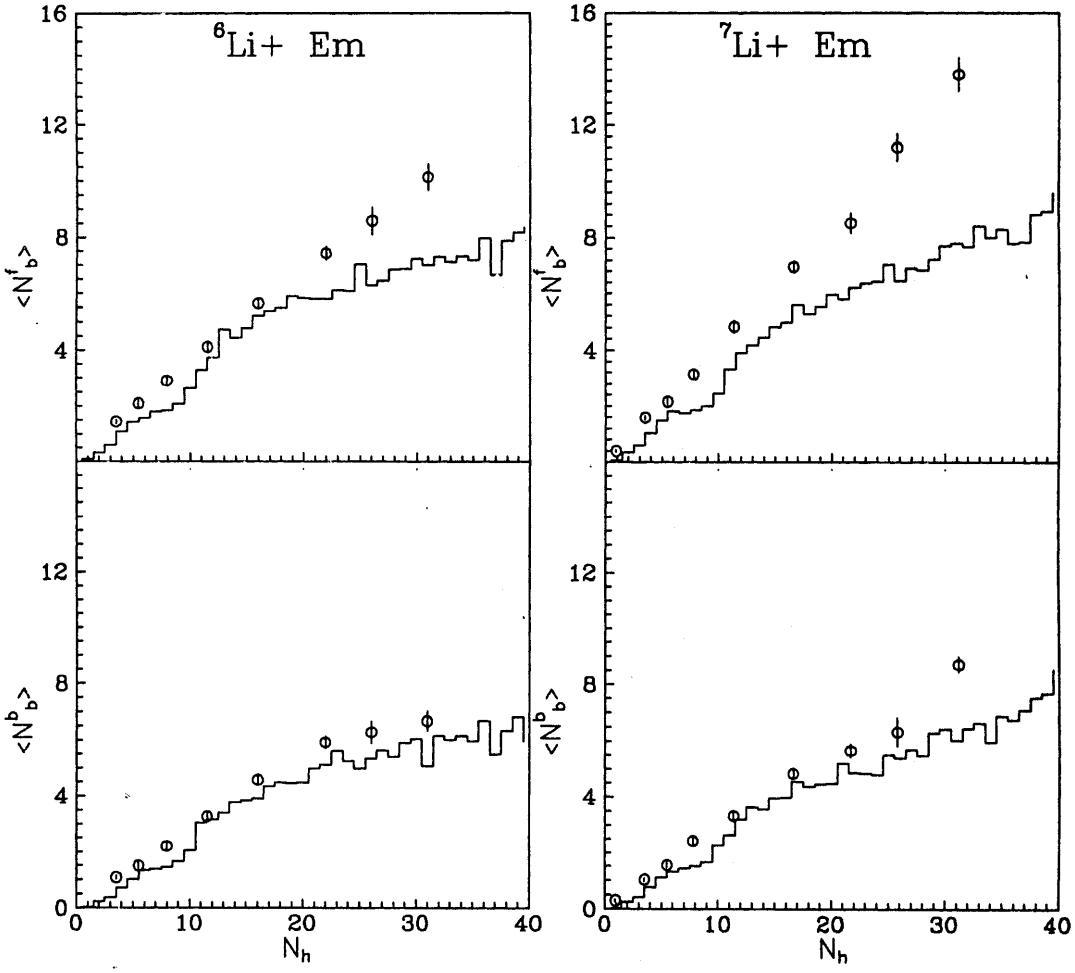

Fig. 5. The dependence of $< N_b^f >$ and $< N_b^b >$ on the average number of heavily ionized tracks N_h. The notation is identical to that in Fig. 2

Table 4. The values of $< N_g^f >$, $< N_g^b >$ and $(F/B)_g$ ratio for spectator projectile charge $Q = 0$, 1, 2, for $^6Li + Em$ and $^7Li + Em$ interactions. The corresponding CEM results are given in parentheses

g-particles			
$^6Li + Em$	$Q = 0$	$Q = 1$	$Q = 2$
$< N_g^f >$	3.51 ± 0.21	2.01 ± 0.26	0.86 ± 0.09
	(8.10)	(2.723)	(1.137)
$< N_g^b >$	1.70 ± 0.09	0.81 ± 0.10	0.41 ± 0.04
	(2.799)	(0.872)	(0.329)
$(F/B)_g$	2.06	2.48	2.08
$^7Li + Em$			
$< N_g^f >$	3.16 ± 0.32	2.55 ± 0.26	1.49 ± 0.03
	(7.695)	(2.764)	(1.143)
$< N_g^b >$	1.37 ± 0.04	0.93 ± 0.10	0.45 ± 0.04
	(2.424)	(0.746)	(0.277)
$(F/B)_g$	2.31	2.74	3.30

Table 5. The same as Table 4 but for b-particles

b-particles			
$^6Li + Em$	$Q = 0$	$Q = 1$	$Q = 2$
$< N_b^f >$	4.47 ± 0.26	2.87 ± 0.41	1.46 ± 0.17
	(3.826)	(1.986)	(0.848)
$< N_b^b >$	3.43 ± 0.13	2.20 ± 0.20	1.20 ± 0.09
	(3.111)	(1.588)	(0.675)
$(F/B)_b$	1.30	1.30	1.22
$^7Li + Em$			
$< N_b^f >$	5.85 ± 0.58	4.43 ± 0.46	2.88 ± 0.27
	(4.165)	(1.912)	(0.833)
$< N_b^b >$	3.91 ± 0.24	2.98 ± 0.21	1.96 ± 0.11
	(3.368)	(1.513)	(0.654)
$(F/B)_b$	1.49	1.49	1.47

– The $(F/B)_g$ ratio decreases with increasing both the centrality and the incident energy.
– In case of ^7Li interactions, the $(F/B)_b$ ratio for b-particles is nearly independent of the projectile spectators which reflects the isotropic behavior of the evaporated b-particles.
– The $(F/B)_{g,b}$ ratios for g and b-particles in case of the interactions induced by ^7Li isotope are higher

Table 6. The values of $< N_g^{f,b} >$, $< N_b^{f,b} >$ and the forward-backward ratios $(F/B)_{g,b}$ for the group of events containing $N_s^b > 0$ and $N_g^b > 0$ in cases of $^6Li + Em$ and $^7Li + Em$ interactions. The corresponding CEM results are given in parentheses

$^6Li + Em$	$< N_g^f >$	$< N_g^b >$	$(F/B)_g$	$< N_b^f >$	$< N_b^b >$	$(F/B)_b$
$N_s^b > 0$	3.84 ± 0.18 (8.180)	1.75 ± 0.11 (2.756)	2.19	4.80 ± 0.20 (3.921)	3.60 ± 0.15 (3.161)	1.33
$N_g^b > 0$	3.41 ± 0.13 (5.434)	2.06 ± 0.07 (2.864)	1.66	4.56 ± 0.15 (3.208)	3.42 ± 0.11 (3.957)	1.33
$^7Li + Em$						
$N_s^b > 0$	3.15 ± 0.17 (7.355)	1.05 ± 0.10 (2.264)	3.00	5.71 ± 0.30 (3.949)	3.57 ± 0.19 (3.184)	1.60
$N_g^b > 0$	3.25 ± 0.13 (4.781)	1.81 ± 0.07 (2.512)	1.80	5.54 ± 0.23 (3.990)	3.63 ± 0.15 (3.224)	1.53

than the corresponding ones in the case of the interactions with ^6Li. This result may be interpreted as due to an increase of cascading with increasing energy. In other words, $(F/B)_g$ decreases with increasing cascading (central interactions) which in turn increases with the increase of the target size, thus increasing B relative to F.

- The CEM reasonably agrees with the measured $< N_g^{f,b} >$ as a function of $Q = 1$, 2, but exceeds the measured values for more central collisions ($Q = 0$). This indicates that the CEM presumes too branched cascade of secondaries at very central collisions than is observed.
- In contrast to the g-particles dependence on Q, the CEM reasonably agrees with the measured $< N_b^{f,b} >$ in the case of central interactions $Q = 0$. But for quasi-central and peripheral interactions ($Q = 1$, 2), the model underestimates the corresponding values.

In Table 6 we present the mean values of the g and b-particles in both hemispheres for the group of events having $N_s^b > 0$ (N_s^b refers to the relativistic hadrons in the BHS) as well as for the events characterized by backward g-particles $N_g^b > 0$. From the Table one can conclude that:

- For any projectile having $N_s^b > 0$, the $(F/B)_{g,b}$ ratios in case of g- and b-particles nearly equal the corresponding values for the total sample of events (compare Table 6 and 3). This could indicate that most of the detected events are characterized by the emission of relativistic hadrons in the BHS.
- The $(F/B)_g$ ratios in case of g-particles having $N_g^b > 0$ nearly equal the values of the isotropy factor for the b-particles. This may imply that the emission of g-particles in such events is nearly isotropic, i.e., the system emitting g-particles nearly have slow velocity as compared to the events having $N_g^b = 0$.
- The mean values of $N_g^{f,b}$ and $N_b^{f,b}$ in the group of events characterized by $N_s^b > 0$ nearly equal the corresponding values for the events having $N_g^b > 0$.
- The dependence of $< N_g^{f,b} >$ and $< N_b^{f,b} >$ on $N_s^b > 0$ or $N_g^b > 0$ is nearly equivalent to the dependence of $< N_g^{f,b} >$ and $< N_b^{f,b} >$ on $Q = 0$. This may show that N_s^b and N_g^b can be used as an indication to the degree of the violence of the collision.

4.6 Multiplicity correlations

From Table 6, it can be seen that the CEM describes the dependence of the average values of g- and b-particles in both hemispheres on $N_g^b > 0$ better than it does on $N_s^b > 0$. Therefore, we will reliably use the former as an indication of the impact parameter dependence. Moreover, the number of backward b-particles is more accurate experimental factor determining the target size dependence than the N_h values. This is because N_b^b is of purely target origin, while N_h contains g-particles which include some contamination (about 10% created slow particles(π, K, ...) at 3.7 A GeV). Thus we will use N_b^b as an indication of purely target events.

4.6.1 Correlations $N_s^{f,b}(N_g^b)$ and $N_s^{f,b}(N_b^b)$

The correlation between g and s-particles are very important due to their mutual dependence on the number of struck nucleons. Moreover, within the model, the protons produced in BHS are mainly due to inelastic NN-interactions with a subsequent production of pions. It can be seen from Fig. 6 that,

- The average numbers of s-particles in the FHS ($< N_s^f >$) sharply increase with increasing the number of backward g-particles up to $N_g^b \sim 4$. This could be due to the fact that in this region ($N_g^b \leq 4$), a superposition of interactions with light and heavy components of emulsion may exist. For higher N_g^b values, an almost constant behavior is observed. Such a trend can be understood by the processes in spectator parts. Starting from $N_g^b > 4$, the interactions on the heavy emulsion nuclei is weakly connected with the process of hadronic production.
- The $< N_s^{f,b} >$ increase with increasing the bombarding energy of the projectile.
- The model fairly reproduces $< N_s^b >$ as a function of N_g^b for the reactions under study.

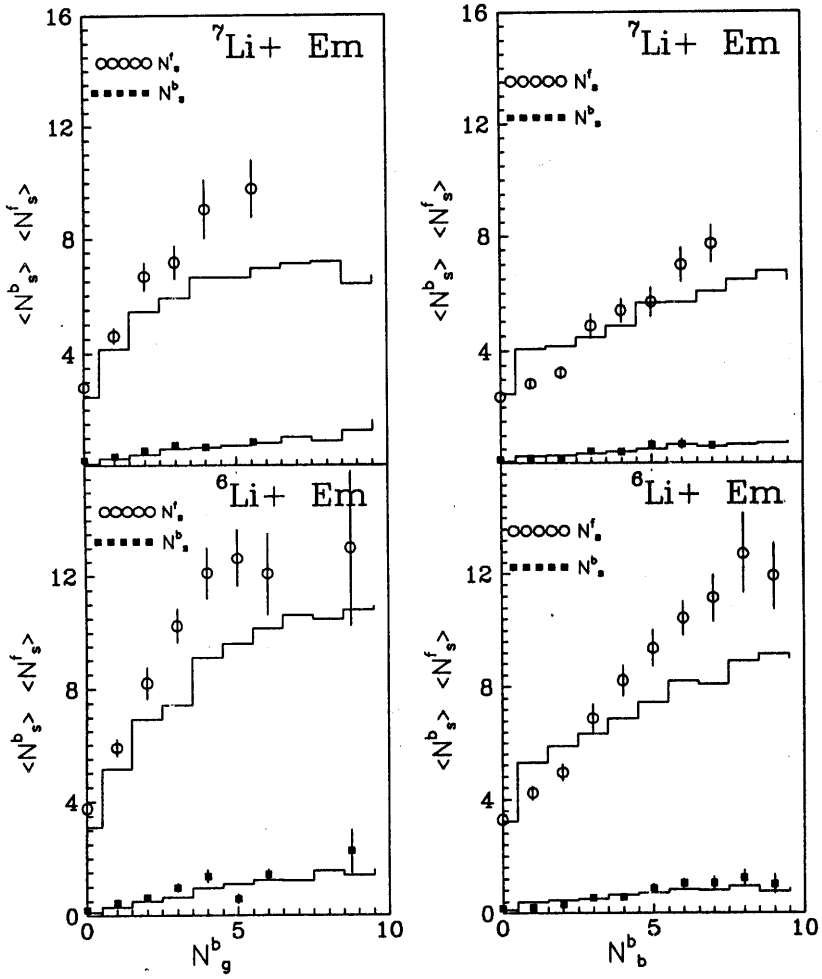

Fig. 6. On the left hand side, the correlations between forward-backward ($< N_s^f >$, $< N_s^b >$) and the backward g-particles (N_g^b). On the right hand side, the dependence of ($< N_s^f >$, $< N_s^b >$) on backward b-particles (N_b^b) for the reactions under study. The notations are the same as in Fig. 2

– In the FHS the model shows the same trend as the data, but predicts small $< N_s^f >$ values for the whole range of N_g^b. This may indicate that: Although the model does not include the formation of Δ-resonance, there are more pion absorption in the nucleus than seen experimentally.

In the same Figure we display the correlation between the average number of s-particles and the multiplicity of b-particles in both hemispheres. In the model, the s-particles are related to the excitation energy of the nucleus (through the dependence of participant nucleons of the two colliding nuclei on cascade particles) and thus in an indirect way to the evaporated b-particles. From the Figure one can see that:

– The model fairly reproduces the dependence of $< N_s^b >$ on N_b^b in the BHS.
– In contrast to the measured correlations where the dependence of $< N_s^f >$ on N_b^b is linear, the calculations show that such variation is rather weak.

From Fig. 6 one can conclude that the $< N_s^{f,b} >$ is strongly correlated with N_g^b than with N_b^b which is also a consequence of the model.

4.6.2 Correlations $N_b^{f,b}(N_g^b)$ and $N_g^{f,b}(N_b^b)$

In the model, the g-particle multiplicity is directly proportional to the total number of participant nucleons in the two nuclei. Moreover, the g-particles contribute to the excitation of the residual nucleus and, therefore, related indirectly to the multiplicity of evaporated b-particles. Thus a study of slow particle production as a function of N_g^b will reveal the impact parameter dependence.

In Fig. 7 we study the dependence of the average number of b-particles in the two hemispheres ($< N_b^{f,b} >$) on the number of backward g-protons N_g^b. By inspection of the Figure we notice that:

– The experimental and calculated values of $< N_b^{f,b} >$ increase with increasing $N_g^b \sim 4$, which turns to a saturation for higher N_g^b values. The saturation seen in

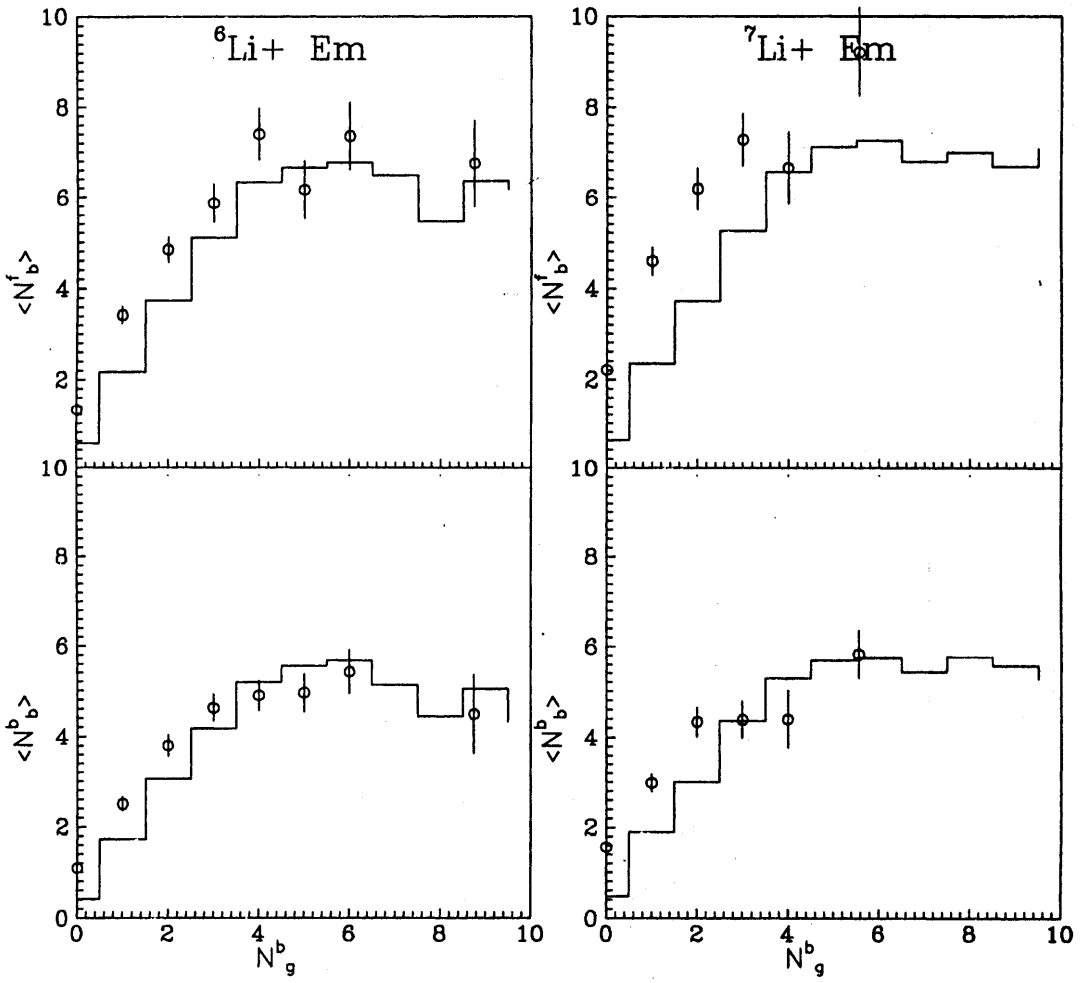

Fig. 7. The dependence of $< N_b^f >$ and $< N_b^b >$ on the number of backward g-particles in the interactions induced by ^6Li(3.7 A GeV) (left hand side) and ^7Li(2.2 A GeV) (right hand side) with emulsion nuclei. The notations are the same as in Fig. 2

$< N_b^{f,b} >$ at medium and small impacts is a consequence of the finite size of the projectile nucleus.
- The model adequately describes the saturation seen in $N_b^{f,b}(N_g^b)$.
- For $N_g^b < 4$, we obtain slightly smaller average b-particles than experimentally observed. Events with $N_g^b < 4$ are dominated by interactions with light nuclei. Again, this is an indication that the Weisskopf's model can not describe the evaporation of light nuclei.

In Fig. 8 we examine the dependence of $< N_g^{f,b} >$ on N_b^b. An increase in the number of backward b-particles N_b^b is accompanied by a fast increase in the multiplicity of forward g-particles ($< N_g^f >$) for the reactions under study. Therefore one can conclude that N_b^b is a good indicator of the target size dependence. The calculations illustrated in Fig. 8 reflect such dependence in a manner stronger than do the experimental data.

4.6.3 Correlations $N_g^f(N_g^b)$ and $N_b^f(N_b^b)$

Finally in Fig. 9 we display the connection between the forward and backward particle production. The model fairly reproduces the dependence of the average b-particles ($< N_b^f >$) on the multiplicity of backward b-particles N_b^b. As for $N_g^f(N_g^b)$, the calculations deviate from the experimental data.

5 Conclusions

From the study of backward slow proton production in the inelastic interaction of ^6Li(3.7 A GeV) and ^7Li(2.2 A GeV) with the emulsion nuclei, the following conclusions can be drawn:

1. The ratio between the number of events with backward g-particles for the $N_h \geq 8$ group and the corresponding number in case of $1 \leq N_h \leq 7$ group is about four.

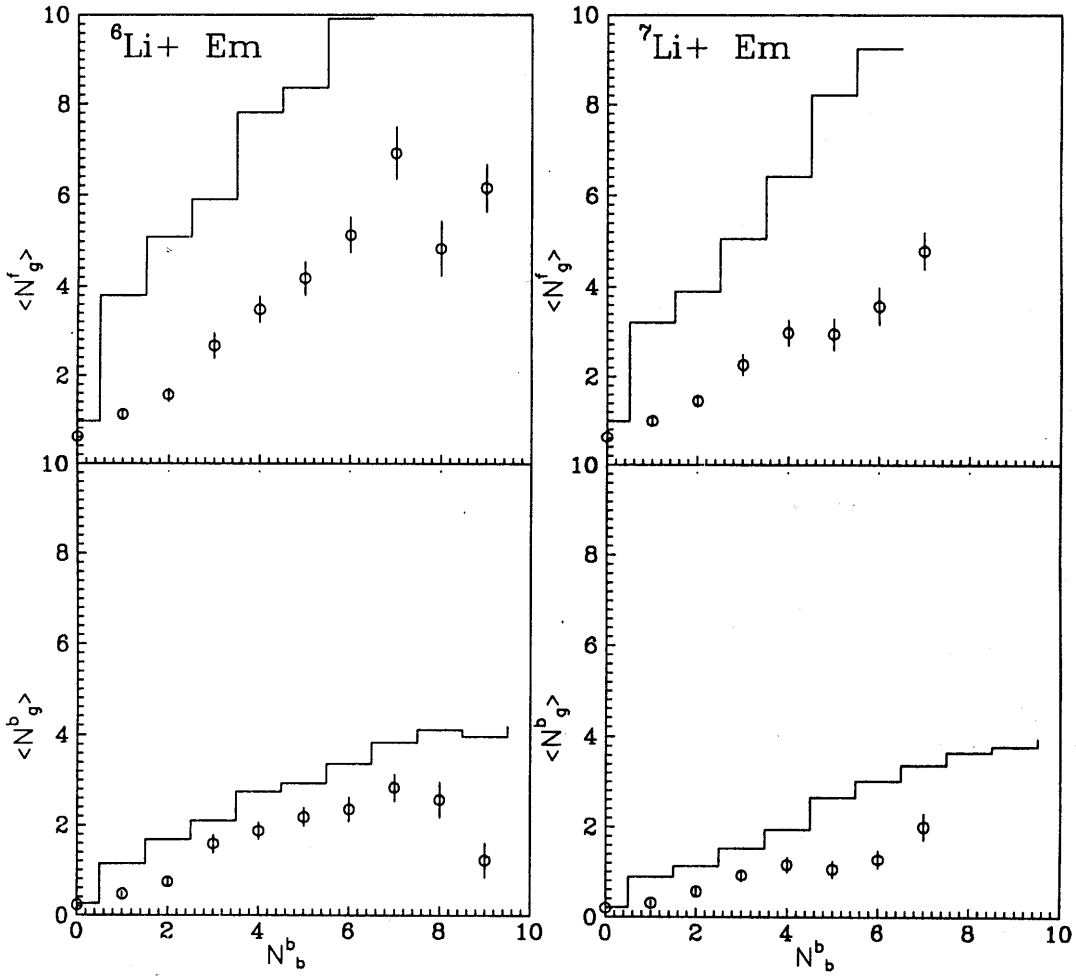

Fig. 8. The dependence of the average number of g-particles produced in the forward and backward hemispheres on the number of backward b-particles for $^6Li + Em$ (left hand side) and $^7Li + Em$ (right hand side). The notations are the same as in Fig. 2

2. The system emitting g-particles in the group of events having $N_g^b > 0$ possesses slow velocity as compared to the ones having $N_g^b = 0$.
3. The backward slow protons N_b^b and N_g^b are good factors determining the purely target events and the impact parameter dependence, respectively.
4. The most central events come from ones having $N_s^b > 0$ or $N_g^b > 0$.
5. The forward to backward ratios $(F/B)_{g,b}$ of g- and b-particles decrease with increasing both the target size and the incident energy.
6. The mechanisms of producing slow protons in the backward and forward hemispheres are different.
7. The CEM shows too much branched cascade of secondary interactions in the very central collisions ($Q = 0$, $N_s^b > 0$ and $N_g^b > 0$).
8. The CEM underpredicts the emission of b-particles multiplicity in both hemispheres for light nuclei.
9. The CEM can describe the correlations between particles emitted in the BHS. On the other hand, for the correlation between backward and forward particles, the model can only predict the b-particles correlation.

In a previous study [31] dealing with the interactions of p, ^4He, ^{12}C, ^{16}O, ^{22}Ne and ^{28}Si with emulsion nuclei at $\sim$ 3 A GeV, it was shown that the CEM describes well the experimental data concerning the total detected N_s, N_g and N_b values. In this work, we have thoroughly examined the production of slow protons in the backward and forward hemispheres. The CEM has shown a good performance only in describing slow protons emitted in the region of limited cascading (BHS). This means that for the FHS, there are problems concerning correct description of particle cascading in nuclei under conditions of strong destruction. Therefore, the present data can be used as a critical check for the modern approaches to describe nuclear cascading ([23]–[26]).

The authors would like to thank Prof. A.M. Baldin and Prof. A.D. Kovalenko from $JINR$ in Dubna for their cooperation in supplying us with the nuclear emulsion plates.

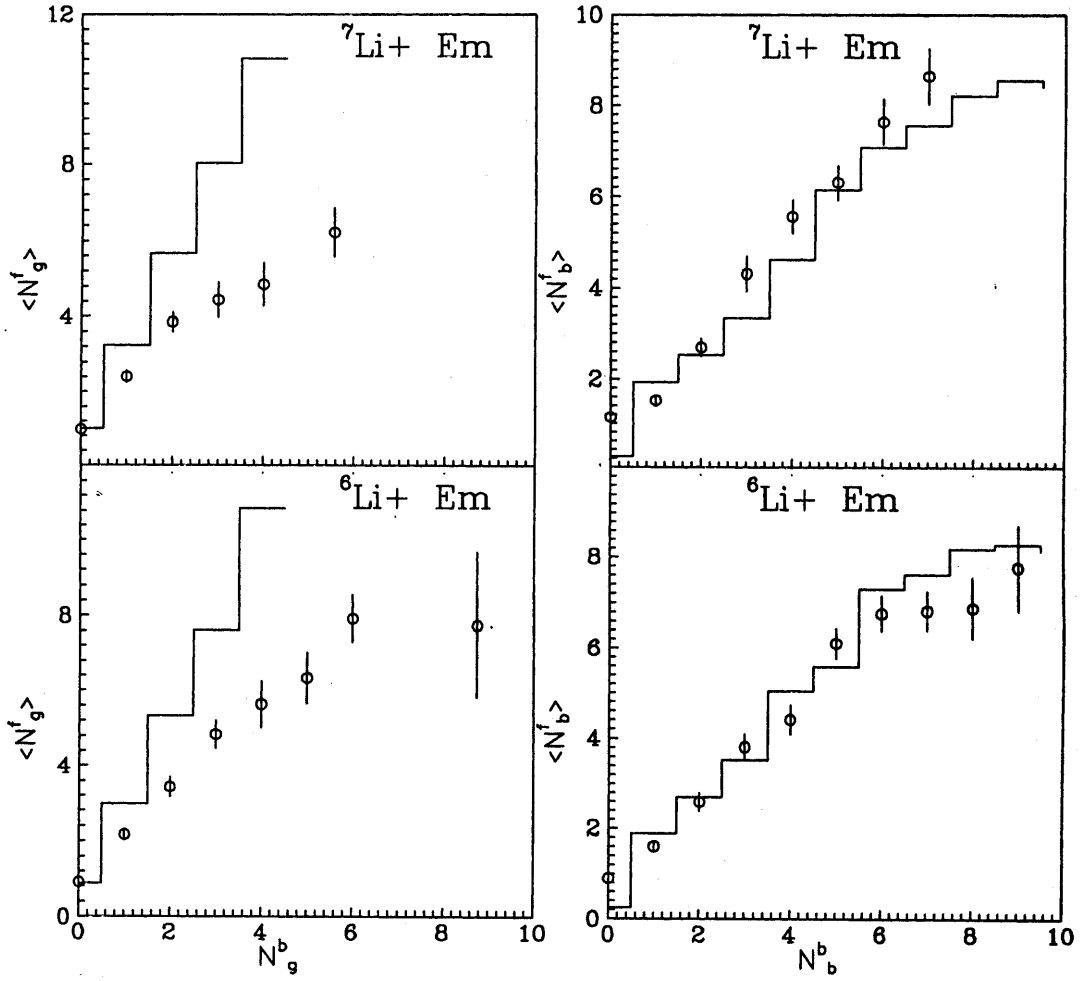

Fig. 9. The correlations between forward (N_g^f) and backward (N_g^b) g-particles in $^6Li + Em$ (bottom) and $^7Li + Em$ (top). On the right hand side, the dependence of forward b-particles (N_b^f) on the backward b-particles (N_b^b) for the reactions under study

References

1. L.S. Schroeder et al., Phys. Rev. Lett. **43**, 1787 (1979)
2. N.A. Burgov et al., Sov. J. Nucl. Phys. **45**(3), 463 (1987)
3. T. Fujita, J. Hufner, Nucl. Phys. **A**314, 317 (1979)
4. J.V Geaga et al., Phys. Rev. Lett. **45**, 1993 (1980)
5. A.M. Baldin et al., Sov. J. Nucl. Phys. **20**(6), 629 (1975)
6. S. Nagamiya et al., Phys. Rev. C **24**, 971 (1981)
7. Y. D. Bayukov et al., Phys. Rev. C **20**, 764 (1979)
8. M. El-Nadi, A. AbdelSalam, N. Ali Moussa, Int. J. Mod. Phys. **E**3, 811 (1994)
9. M. El-Nadi, N. Ali-Moussa, A. AbdelSalam, accepted for publication in IL Nuovo Cimento (1997)
10. A. AbdelSalam, M. Sumberg, S. Vokal, JINR, E1-82-509 (Dubna 1982) and Int. Conf. On Nucl.-Nucl. Interactions (Michigan 1982)
11. V.S. Barachenkov, F.G. Zheregi, Zh.Zh. Musulmanbekeov, preprint of JINR, R2-83-117, Dubna, 1983
12. V.D. Toneev, K.K. Gudima, Nucl. Phys. A **400**, 173 (1983); ibid, A **401**, 329 (1983)
13. V. Weisskopf, Phys. Rev. **52**, 295 (1937)
14. M. El-Nadi et al., Il Nuovo Cimento **107A**, 31 (1994)
15. M. El-Nadi et al., Egypt. J. of Phys. **24**, 49 (1993)
16. M. El-Nadi et al., Egypt. J. of Phys. **24**, 101 (1993)
17. S.Yu. Shmakov, V.V. Uzhinskii, A.M. Zadorozhny, Comput. Phys. Comm. **54**, 125 (1989)
18. M. Blann, Rev. Nucl. Sci. **17**, 478 (1966)
19. W.A. Friedman, Phys. Rev. **C28**, 16 (1983)
20. I. Dostrovsky, Z. Frankel, G. Friedlandel, Phys. Rev. **116**, 683 (1959)
21. V.S. Barachenkov, K.K. Gudima, V.D. Toneev, Acta Phys. Pol. **36**, 260 (1969)
22. V.S. Barachenkov et al., Nucl. Phys. A **187**, 531 (1972)
23. S.G. Mashnik, *Proc. of a specialists meetings intermediate energy nuclear data* Models and Codes, Paris (1994) 107
24. V.D. Toneev, K.K. Gudima, preprint of GSI, Darmstadt, GSI-93-52 (1993)
25. G.O. Dorso, P.E. Balonga, Phys. Rev. **C**50, 991 (1994)
26. A. Ferrari, J. Ranft, S. Roesler, P.R. Sala, Z. Phys. **C**70, 431 (1996)
27. J.R. Florian et al., Phys. Rev. D **13**, 558 (1976)
28. N. Angelave et al., Sov. J. Nucl., Phys. **32** (1980)
29. E. Fermi, Prog. Theor. Phys. **5**, 1570 (1950)
30. A. AbdelSalam, Physica Scripta **47**, 505 (1993)
31. V.V Uzhinskii, A.S. Pak, Phys. of Atomic Nuclei, **59**, 1064 (1996)